Metabolism and Bioenergetics:

Biochemical and Structural Insights into Bacterial Organelle Form and Biogenesis

Joshua B. Parsons, Sriramulu D. Dinesh, Evelyne Deery, Helen K. Leech, Amanda A. Brindley, Dana Heldt, Steffanie Frank, C. Mark Smales, Heinrich Lünsdorf, Alain Rambach, Mhairi H. Gass, Andrew Bleloch, Kirsty J. McClean, Andrew W. Munro, Stephen E. J. Rigby, Martin J. Warren and Michael B. Prentice

J. Biol. Chem. 2008, 283:14366-14375.
doi: 10.1074/jbc.M709214200 originally published online March 10, 2008

THE JOURNAL OF BIOLOGICAL CHEMISTRY VOL. 283, NO. 21, pp. 14366–14375, May 23, 2008

Biochemical and Structural Insights into Bacterial Organelle Form and Biogenesis*[S]

Received for publication, November 9, 2007, and in revised form, March 10, 2008 Published, JBC Papers in Press, March 10, 2008, DOI 10.1074/jbc.M709214200

Joshua B. Parsons[‡1], Sriramulu D. Dinesh[§1], Evelyne Deery[‡], Helen K. Leech[‡], Amanda A. Brindley[‡], Dana Heldt[‡], Steffanie Frank[‡], C. Mark Smales[‡], Heinrich Lünsdorf[¶], Alain Rambach[‖], Mhairi H. Gass[**], Andrew Bleloch[**], Kirsty J. McClean[‡‡], Andrew W. Munro[‡‡], Stephen E. J. Rigby[§§], Martin J. Warren[‡2], and Michael B. Prentice[§3]

From the [‡]Protein Science Group, Department of Biochemistry, University of Kent, Canterbury, Kent CT2 7NJ, United Kingdom, [§]Departments of Pathology and Microbiology, University College Cork, Cork, Ireland, [¶]Department of Vaccinology, Helmholtz Center of Infection Research, Braunschweig D-38124, Germany, [‖]CHROMagar, 4 place du 18 Juin 1940, F-75006 Paris, France, [**]SuperSTEM Facility, Daresbury Laboratories, Daresbury WA4 4AD, United Kingdom, [‡‡]Faculty of Life Sciences, Manchester Interdisciplinary Biocentre, University of Manchester, 131 Princess Street, Manchester M1 7DN, United Kingdom, and [§§]School of Biological and Chemical Sciences, Queen Mary, University of London, Mile End Road, London E1 4NS, United Kingdom

Many heterotrophic bacteria have the ability to make polyhedral structures containing metabolic enzymes that are bounded by a unilamellar protein shell (metabolosomes or enterosomes). These bacterial organelles contain enzymes associated with a specific metabolic process (*e.g.* 1,2-propanediol or ethanolamine utilization). We show that the 21 gene regulon specifying the *pdu* organelle and propanediol utilization enzymes from *Citrobacter freundii* is fully functional when cloned in *Escherichia coli*, both producing metabolosomes and allowing propanediol utilization. Genetic manipulation of the level of specific shell proteins resulted in the formation of aberrantly shaped metabolosomes, providing evidence for their involvement as delimiting entities in the organelle. This is the first demonstration of complete recombinant metabolosome activity transferred in a single step and supports phylogenetic evidence that the *pdu* genes are readily horizontally transmissible. One of the predicted shell proteins (PduT) was found to have a novel Fe-S center formed between four protein subunits. The recombinant model will facilitate future experiments establishing the structure and assembly of these multiprotein assemblages and their fate when the specific metabolic function is no longer required.

It has been recognized for more than 30 years that all cyanobacteria (1) and some other chemoautotrophic bacteria (2) contain carboxysomes. These polyhedral cellular inclusions consist of a proteinaceous shell enclosing an active enzyme, ribulose bisphosphate carboxylase/oxygenase (RuBisCO).[4] Their function is to enhance the fixation of carbon dioxide (3), a reaction of planetary significance in that marine cyanobacteria are responsible for the majority of global carbon fixation (4, 5). More recently, sequence similarity was noticed between carboxysome shell genes and metabolic operon genes associated with propanediol utilization (*pdu*) and ethanolamine utilization (*eut*) in a variety of heterotrophic bacteria found in the mammalian gut (3) and the environment. In growth conditions that induce these metabolic operons, polyhedral organelles resembling carboxysomes were observed on electron microscopy of *Salmonella enterica* serovar Typhimurium (6), *Klebsiella oxytoca, Citrobacter freundii*, and *Escherichia coli* (7). Bioinformatics analysis also locates genes resembling carboxysome shell genes in metabolic operons in *Clostridium perfringens* (8), *Clostridium tetani* (9), *Listeria monocytogenes* and *Listeria innocua* (10), *Enterococcus faecalis* (11), *Lactobacillus collinoides* (12), *Citrobacter rodentium*,[5] and *Yersinia enterocolitica* (13) among other organisms. The non-carboxysome polyhedral structures have been referred to as enterosomes (3) or metabolosomes (14), emphasizing their role in cellular metabolism.

There is some considerable interest in how these proteinaceous organelles form and the arrangement of protein subunits that give rise to these remarkable macromolecular assemblies. In carboxysomes, there are thought to be a number of shell proteins that encase the RuBisCO and carbonic anhydrase. The situation is more complex in metabolosomes, where there are at least five shell proteins that encase ancillary factors, metabolic enzymes, and activating factors. There are thus between 17 and 21 genes associated with the ethanolamine and propanediol metabolosomes, respectively, and although some functional studies have been undertaken, little is known about the topological arrangement of the encoded protein components within the organelle. However, sequence analysis reveals that the shell proteins found in carboxysomes and metabolosomes are similar, indicating that they have evolved from a common ancestor.

* This work was supported by the Science Foundation Ireland (Research Frontiers Programme 05-RF-GEN053) and the Biotechnology and Biological Sciences Research Council. The costs of publication of this article were defrayed in part by the payment of page charges. This article must therefore be hereby marked "*advertisement*" in accordance with 18 U.S.C. Section 1734 solely to indicate this fact.

[S] The on-line version of this article (available at http://www.jbc.org) contains supplemental Figs. S1–S3 and Tables S1 and S2.

The nucleotide sequence(s) reported in this paper has been submitted to the GenBank™/EBI Data Bank with accession number(s) AM498294.

[1] These authors contributed equally to this work.

[2] To whom correspondence may be addressed. Tel.: 44-1227-824690; E-mail: m.j.warren@kent.ac.uk.

[3] To whom correspondence may be addressed. Tel.: 353-21-4901420; E-mail: m.prentice@ucc.ie.

[4] The abbreviations used are: RuBisCO, ribulose bisphosphate carboxylase/oxygenase; FFT, fast Fourier transformation; MALDI-TOF, matrix-assisted laser desorption ionization time-of-flight.

[5] M. Prentice, unpublished material.

Structural studies on some of the individual shell proteins have given an insight into how they may function. The main carboxysome shell protein, CCMK1, has been shown to have a hexameric crystal structure with a charged pore (15), suggesting a selective permeability mechanism making the structure a prokaryotic functional equivalent to a eukaryotic organelle. Structures of the CsoS1A carboxysome protein from *Halothiobacillus neapolitanus* (16) and the EutN shell protein of the ethanolamine utilization enterosomes from *E. coli* (17) also reveal similar hexameric arrangements with charged residues surrounding a central pore. Cryoelectron microscopy of extracted carboxysomes shows they have an icosahedral symmetry with triangular faces, but a complete image reconstruction was not possible because of a variability in individual carboxysome size, lack of symmetry in carboxysome contents, and absence of obvious capsomers on the surface (18). A similar imaging project has provided even further detail, suggesting that carboxysomes isolated from a *Synechococcus* strain contain ~250 RuBisCOs, which are organized into three or four concentric layers (19).

The distribution and relatedness of both the structural genes for the protein shell (15) and the associated metabolic operons (20, 21) strongly suggest repeated horizontal transmission in evolution. In keeping with this, we show that plasmid-based expression in *E. coli* of a *pdu* operon from *C. freundii* containing metabolosome structural and enzyme genes results in synthesis of recombinant metabolosomes with fully functional enzyme activity. In this way we have compartmentalized the bacterial cytoplasm, showing that it is possible to create novel compartments by horizontal genetic transfer in bacteria and to vary the shape and topology of the organelle by overproducing individual shell proteins. This process has the potential to be used for metabolic engineering whereby bacteria can be shielded from toxic metabolic intermediates. Thus, this project will contribute to the emerging discipline of synthetic biology.

EXPERIMENTAL PROCEDURES

A more detailed account of the techniques, including the cloning and sequencing of the *pdu* operon is given in the supplemental material.

Citrobacter sp. Library—The genomic DNA of *Citrobacter sp*. was partially digested with Sau3AI, and 20–30-kb fragments were purified after separation by agarose gel electrophoresis, cloned into the BglII site of the cosmid pLA 2917, and encapsidated *in vitro* following the Packagene® Lambda DNA packaging system instructions (Promega). The library was used to infect *E. coli* LE392. One cosmid, which had the ability to degrade 1,2-propanediol, was isolated and named pAR3114 (supplemental Table S1).

Bacteria and Growth Conditions—All strains and plasmids are described in supplemental Table S1. *E. coli* JM109 wild-type and recombinant strains harboring pLA2917 (22) and pAR3114 were grown either in LB medium or trypticase soy agar (10 g of tryptone, 5 g of NaCl, and 15 g of agar in 1 liter of distilled water) without or with tetracycline (20 μg/ml), respectively. pAR3114 is a pLA2917 cosmid containing an ~30-kb (*pdu* operon, *cbi*A and *poc*R genes) insert derived from Sau3AI digestion of the *C. freundi* chromosome.

Sequencing of Insert, Gene Annotation, and Recombinant Manipulation—The *pdu* operon sequence was obtained from pAR3114 after it was sent to be sequenced by Qiagen Ltd. The insert was found to contain 28,618 bp. The sequencing coverage was higher than 12, and the data quality has an error rate of $<1/10000$ bp and a base accuracy of $>99.99\%$. The cloning and overproduction of individual Pdu components was achieved as described in the supplemental material.

Propanediol Utilization Assay—The utilization of 1,2-propanediol was tested by a MacConkey triple-plate method (20). Bacteria were streaked on to MacConkey agar (20 g Soy peptone, 5 g of ox bile, 5 g of NaCl, 0.075 g of neutral red, 1% 1,2-propanediol, and 12 g of agar in 1 liter of distilled water) plates containing 1,2-propanediol, 20 μM cobalt chloride, or 100 nM cobinamide. Plates were incubated at 37 °C for 24 h. Formation of red colonies indicated the utilization of 1,2-propanediol by the reduction in pH due to the formation of propionate, and a more rapid appearance of red color with the addition of cobinamide indicated cobalamin dependence of propanediol utilization.

Isolation of Metabolosomes—Metabolosomes were isolated by the organelle purification procedure as described previously (7) and outlined further in the supplemental material.

Electron Microscopy—Late logarithmic phase cells of *E. coli* pLA2917 and pAR3114 were prefixed in 2.5% (v/v) glutardialdehyde, 10 mM Hepes, pH 7.0, for 72 h. After immobilization in 2% (w/v) water-agar they were postfixed in 1% (w/v) osmium tetroxide in 75 mM cacodylate, pH 7.2, for 60 min at 4 °C followed by dehydration in an ethanol series. The 70% dehydration step, supplemented with 1% (w/v) uranylacetate, was done overnight at ambient temperature following the method of Bobik *et al.* (6). Ultrathin sections (90 nm) were post-stained with 4% (w/v) aqueous uranylacetate and analyzed at zero-loss bright field mode in an energy-filtered transmission electron microscope (Zeiss CEM 902, Oberkochen, Germany).

Isolated polyhedral bodies were fixed in 1% (v/v) glutardialdehyde, and after adsorption to Formvar-carbon-coated grids they were negatively stained with 2% (w/v) uranylacetate, pH 4.5. Samples were analyzed by energy-filtered transmission electron microscope, and images were recorded, in general, with a charge-coupled device camera (CCD; Proscan Electronic Systems, Scheuring, Germany). Fast Fourier transformations (FFT) of individual particles was done with CRISP software (Calidris, Sollentuna, Sweden).

SuperSTEM microscopy was carried out on a VG HB501 dedicated STEM fitted with a Nion second generation spherical aberration corrector, high angle annular dark field detector (angular range 70–210 mrad), and a Gatan Enfina electron energy loss spectrometer.

Diol Dehydratase Assay—The activity of diol dehydratase was measured by the 3-methyl-2-benzothiazolinone hydrazone method as described previously (23). One unit of diol dehydratase activity is defined as the amount of enzyme that catalyzes the formation of 1 μmol of propionaldehyde/min/mg of protein.

EPR Analysis and Redox Potentiometry—Continuous wave EPR spectra were recorded on a Bruker Elexis E500/580 spectrometer operating at X-band (9.7 MHz) equipped with an Oxford helium flow cryostat as described previously. Redox

TABLE 1
Genes present on pAR3114, a cosmid containing a 30-kb insert of *C. freundii* genomic DNA

Gene	Start	End	Function	Length	Direction of transcription	Predicted mass
				bp		*Da*
cbiB	835	1	Cobalamin biosynthesis protein	834	−	17,817
cbiA	2,211	832	Cobyrinic acid *a,c*-diamide synthase	1379	−	49,669
pocR	3,718	2,807	Transcriptional regulator	911	−	49,636
pduF	4,729	3,920	Propanediol diffusion facilitator	809	−	28,125
pduA	5,255	5,532	Shell protein	277	+	9,376
pduB	5,536	6,348	Shell protein	812	+	28,021
pduC	6,367	8,031	Diol dehydratase large subunit	1664	+	60,280
pduD	8,042	8,716	Diol dehydratase medium subunit	674	+	24,280
pduE	8,731	9,249	Diol dehydratase small subunit	518	+	19,233
pduG	9,265	11,097	Diol dehydratase reactivation protein	1832	+	64,163
pduH	11,087	11,437	Diol dehydratase reactivation protein	350	+	12,632
pduJ	11,457	11,732	Shell protein	275	+	9,053
pduK	11,823	12,227	Shell protein	404	+	13,921
pduL	12,227	12,859	Phosphotransacylase	632	+	23,048
pduM	12,856	13,347	Unknown	491	+	18,175
pduN	13,351	13,626	Shell protein	275	+	9,205
pduO	13,635	14,642	Cobalamin adenosyltransferase	1007	+	45,886
pduP	14,639	16,024	CoA-dependent propionaldehyde dehydrogenase	1385	+	48,671
pduQ	16,035	17,147	Propanol dehydrogenase	1112	+	39,702
pduS	17,144	18,499	Cobalamin reductase	1355	+	48,568
pduT	18,502	19,056	Shell protein	554	+	19,038
pduU	19,056	19,406	Shell protein	350	+	12,483
pduV	19,411	19,863	Unknown	452	+	16,331
pduW	19,848	21,062	Propionate kinase	1214	+	43,634
pduX	21,092	22,021	Unknown	929	+	33,908
yeeA	23,694	22,636	Putative inner membrane protein	1058	−	39,618
DacD	25,544	24,372	DD-carboxypeptidase	1172	−	43,085
phsC	26,450	25,683	Thiosulfate reductase cytochrome B subunit	767	−	28,545
phsB	27,035	26,456	Thiosulphate reductase protein	579	−	21,622
phsA	28,618	27,043	Thiosulphate reductase precursor	1575	−	53,778

titrations were performed in a Belle Technology glove-box under a nitrogen atmosphere, essentially as described previously (24, 25).

RESULTS

Utilization of 1,2-Propanediol—Transformation of *E. coli* JM109 cells with a cosmid library made from a partial digest of the *C. freundii* genome resulted in the identification of a single red colony when the library was plated on propanediol-MacConkey medium (PM medium). The appearance of this red colony was likely due to the ability of the recombinant strain to metabolize 1,2-propanediol, a phenotype absent in wild-type *E. coli*. The cosmid, termed pAR3114, was found to house an ~30 kb insert. The insert was sequenced, which revealed that it encoded 30 contiguous genes involved in cobalamin biosynthesis and propanediol utilization and five other genes localized at one end of the insert. These genes and the putative functions of the encoded protein products are described in Table 1. The sequence data have been deposited in the EMBL Nucleotide Sequence Database under accession number AM498294.

Gene Order and Similarity to S. enterica—The *C. freundii pdu* genes constitute a probable regulon, comprising a 21-gene operon and a regulatory gene. The gene order was found to be identical to that previously reported in *S. enterica* (6), forming a divergent operon with the *cbi* operon for cobinamide synthesis from a central regulatory gene, *pocR* (Fig. 1*a*).

Subcloning of the pdu Operon—E. coli pAR3114 formed *red* colonies on the PM plate in the presence of cobinamide, whereas it remained *yellow* in its absence indicating the requirement of B_{12} for propanediol metabolism (Fig. 1*b*). The *E. coli* pLA2917 vector control strain formed *yellow* colonies on PM agar with cobinamide, showing its inability to metabolize 1,2-propanediol.

The insert within pAR3114 was trimmed in size by deleting the *cbiB*, *cbiA*, *pocR*, and *pduF* genes upstream of the main *pdu* operon, and a further five genes downstream of the *pdu* operon that are transcribed in the opposite direction and are not thought to be associated with the *pdu* operon (see Table 1). This shortened insert, containing just the 21 genes of the *pdu* operon, was cloned into pET14 generating plasmid pED460. When transformed into JM109, bacterial colonies turned red when grown on PM indicator plates, demonstrating that the transformed bacteria had gained the ability to metabolize propanediol. A further deletion was made whereby *pduA* and *pduB* were removed from the insert in pED460 to give pED461 (supplemental Table S1). The resulting plasmid, when transformed into *E. coli* JM109, had a greatly reduced ability to metabolize propanediol on PM medium in that the colonies turned only slightly pink. Reconstitution of propanediol metabolism was achieved by adding *pduA-B* back in *trans* on a separate, compatible plasmid (pLysS). However, the individual addition of either *pduA* or *pduB* did not restore propanediol metabolism, demonstrating that both proteins are required for this activity.

Electron Microscopy—Cobalamin-dependent propanediol utilization is associated with the formation of intracellular inclusions called carboxysome-like bodies, enterosomes, or metabolosomes (6). We therefore examined our transformed cells for evidence of metabolosomes. Ultrathin sections of *E. coli* pAR3114 grown on minimal medium in the presence of 1,2-propanediol showed intracellular metabolosomes (Fig. 2*b*). *E. coli* pLA2917 (empty cosmid) control strain grown on mini-

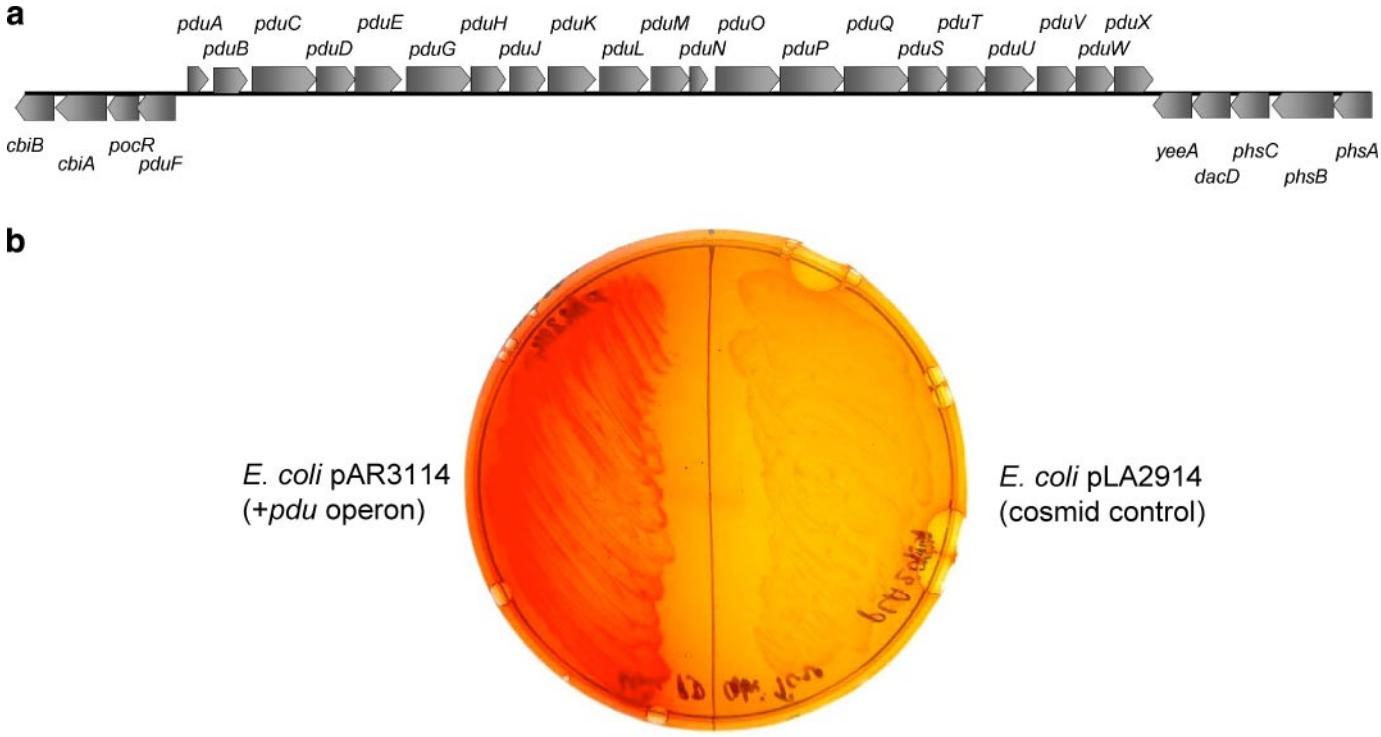

FIGURE 1. **Gene organization on the insert found in pAR3114 and the effect the cosmid has on propanediol utilization when transformed into *E. coli*.** *a*, the order and direction of the genes found on the insert in pAR3114 are shown. The length of the *arrow* provides an approximate relative size of each of the genes. The putative function of encoded proteins are described in Table 1. *b*, *E. coli* strains transformed with pAR3114 and pLA2914 grown on MacConkey agar containing 1% 1,2-propanediol and 100 nM cobinamide for 18 h at 37 °C. The *red* coloration observed with the transformant with pAR3114 is consistent with its ability to produce propionic acid.

mal medium in the presence of 1,2-propanediol did not show metabolosomes inside the cells (Fig. 2*a*). When grown on rich medium (LB), *E. coli* pAR3114 contained metabolosomes in the presence or absence of added propanediol. In cells grown on rich medium, the metabolosomes were closely packed and formed up to 90% of the observed section surface. Again, control strains containing the empty cosmid did not reveal any such structures when grown under similar conditions.

In ultrathin cell sections, the metabolosomes measured on average 101 nm across their widest diameter ($n = 63$; S.D. = 25 nm). There were two maxima in the frequency distribution of measured diameters, compatible with two different size bodies or different sections of a non-spherical polyhedral structure with shorter (77–92 nm) and longer (108–123 nm) axial dimensions (Fig. 2*d*). These dimensions are similar to those reported for wild-type metabolosomes formed in *S. enterica* (7), and carboxysomes from *H. neapolitanus* also show variable sizes with two distinct maximal diameters (18). When looked at in detail (Fig. 2*c*, *white arrows*), apparent sections of polyhedral bodies showed a weak linearly ordered substructure, indicating a certain degree of interior package order. Additionally, polar deposits of electron-dense amorphous granules could be observed in many recombinant cells (Fig. 2*b*, *asterisks*).

When the *E. coli* strain containing the *pdu* operon, but missing *pduA-B*, was analyzed by electron microscopy, no metabolosomes were observed (data not shown). Metabolosomes were observed again when this strain was complemented with a compatible plasmid containing *pduA-B* (data not shown). However, no organelles or other structures were seen in strains in which only *pduA* or *pduB* was added back in *trans* (data not shown). This result indicates that both PduA and PduB are required for organelle biogenesis. Previous research on the *S. enterica pdu* operon had shown that PduA is essential for organelle formation (26).

Diol Dehydratase Activity—The activity of diol dehydratase was measured from the protein extracted from *E. coli* pAR3114 grown to stationary phase in the presence and absence of 1,2-propanediol. Diol dehydratase activity was detected at 2.23 units/mg whole-cell protein for *E. coli* pAR3114 grown in the presence of 1,2-propanediol. Activity was reduced to 0.72 unit/mg when *E. coli* pAR3114 was grown in the absence of 1,2-propanediol. Recombinant metabolosomes were extracted from cells grown in minimal medium with propanediol as per published methods for the extraction of wild-type metabolosomes (7). Purified metabolosomes derived from *E. coli* pAR3114 grown in the presence of 1,2-propanediol showed diol dehydratase activity of 32.03 units/mg protein, ~14 times higher than the enzyme activity found in the crude protein extract.

Extracted Polyhedral Metabolosomes—Metabolosomes were purified from *E. coli* pAR3114 as described under "Experimental Procedures" and in the supplemental material and were viewed both by an energy-filtered transmission electron microscope in the elastic bright field mode and a novel aberration-corrected non-contrast electron microscopy technique using a SuperSTEM instrument. No such structures were obtained from *E. coli* control strains, indicating that the metabolosomes were generated as a result of the presence of the *pdu* operon. The interior of negatively stained polyhedral bodies of *E. coli* pAR3114, fixed with glutardialdehyde (Fig. 3*a*), showed a finely

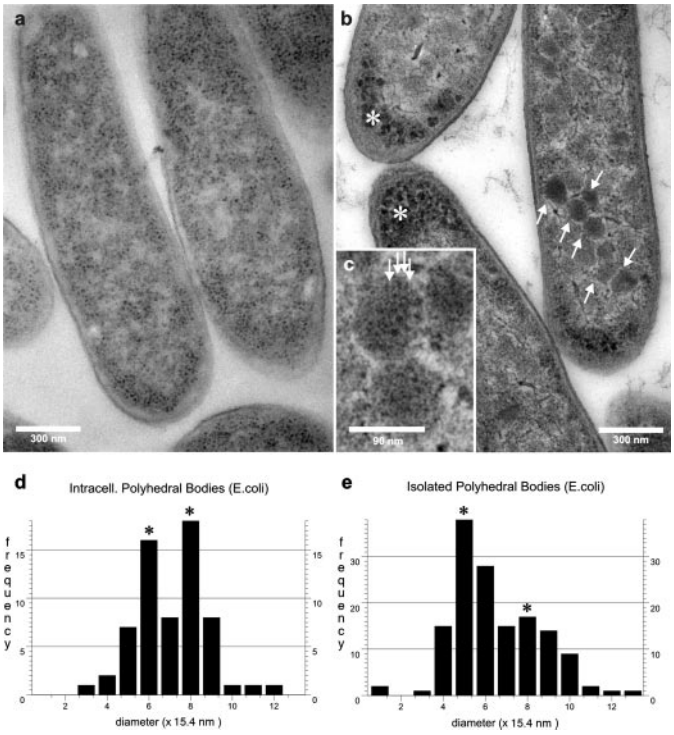

FIGURE 2. **Electron micrographs of wild-type and *pdu*-engineered *E. coli*.** *a*, detailed survey view of *E. coli* (pLA2917) with normally structured cytoplasm panel. *b*, *E. coli* (pAR3114) with the cytoplasm densely packed with metabolosome bodies (*white arrows*). Some granular dense matter of unknown specificity is deposited near the polar ends of the cells (*white asterisks*). *c*, enlarged view of polyhedral bodies from *panel b* that show some regular substructure (*white arrows*). *d* and *e*, diagrams of diameter (minima and maxima) measurements for metabolosome bodies found intracellularly (*d*) and after isolation from lysed *E. coli* cells followed by ultracentrifugation (*e*). The diagrams show two frequency maxima in each histogram, which indicate mean width over length distribution (*asterisks*).

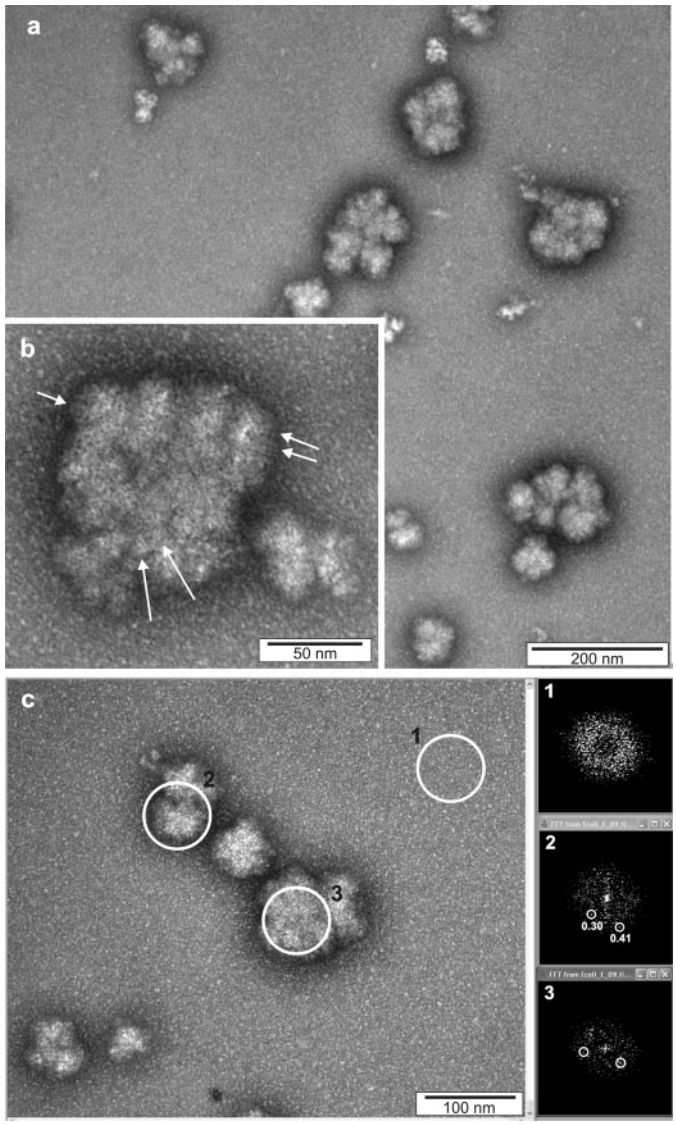

FIGURE 3. **Survey view of isolated polyhedral bodies from *E. coli* (pAR3114).** *a*, electron micrograph of the isolated metabolosomes. The internal organization of all the particles has an irregular or fragmented geometric appearance. *b*, polyhedral bodies show subpatterns of regular, linearly ordered substructures (*arrows*), which appears microcrystalline. The line spacing is about 7 nm. *c*, FFT measurements on background (*1*) and polyhedral bodies (*2* and *3*) and their corresponding power spectra (128 × 128 matrices). As shown on FFT 2, weak intensity spots at 0.30 and 0.41 1/nm frequencies are obvious, which indicates structural internal order. No such intensity spots are observed in FFT 1 of the negative stain background.

branching substructure. These particles had a mean diameter of 92 nm ($n = 143$; S.D. = 32 nm) with a frequency distribution showing 1 maxima (presumed short axis) from 62 to 77 nm and a presumed long axis from 108 to 123 nm (Fig. 2*e*). Higher magnifications of those particles showed regularly arranged substructures with a layer spacing of about 7 nm (Fig. 3*b*, *white arrows*). Intrinsic order on or below this scale within isolated polyhedral bodies was detected by FFT (Fig. 3*c*, *FFTs 2* and *3*) relative to the amorphous foil substratum (Fig. 3*c*, *FFT 1*) Distinct frequency intensities within a 128 × 128 matrix were obvious at 0.30 and 0.41 per nm, corresponding to a particulate resolution of 3.3 and 2.4 nm (Fig. 3*c*, *FFT 2*). That is, the electron micrographs shown resolve structures as small as 2.4 nm, confirming their ability to detect 7-nm layers.

Further evidence for regular metabolosome substructure was obtained using SuperSTEM microscopy of the recombinant metabolosomes both in cell sections and protein extracts. A number of particles displayed apparent multicomponent substructure, with smaller particles containing electron density typical of proteins (Fig. 4, *a* and *b*). This suggests that the interior of the metabolosome is not an amorphous mixture of component molecules but constitutes a regular assembly of structural proteins. Such a regular assembly has recently been reported for carboxysomes from *Synechocystis*, where the RuBisCOs are organized into three or four concentric layers (19). Currently crystal structures of carboxysome and metabolosome shell proteins show them forming flat hexagonal sheets, although it has not been determined how this planar structure can bend or fold up to form a closed shell (15, 16). Our SuperSTEM images showing discrete electron-dense foci spaced around the recombinant metabolosomes suggest the presence of non-planar protein complexes acting as structural linkage points joining sheets of shell protein to form the faceted surface of the metabolosome (Fig. 4, *c* and *d*) in the same way that vertex proteins link planar proteins to form the viral capsid structure (27, 28). As in viral capsids, these complexes are presumably pentameric, connecting planes of hexameric shell proteins (27, 28). The likely candidate for this metabolosome com-

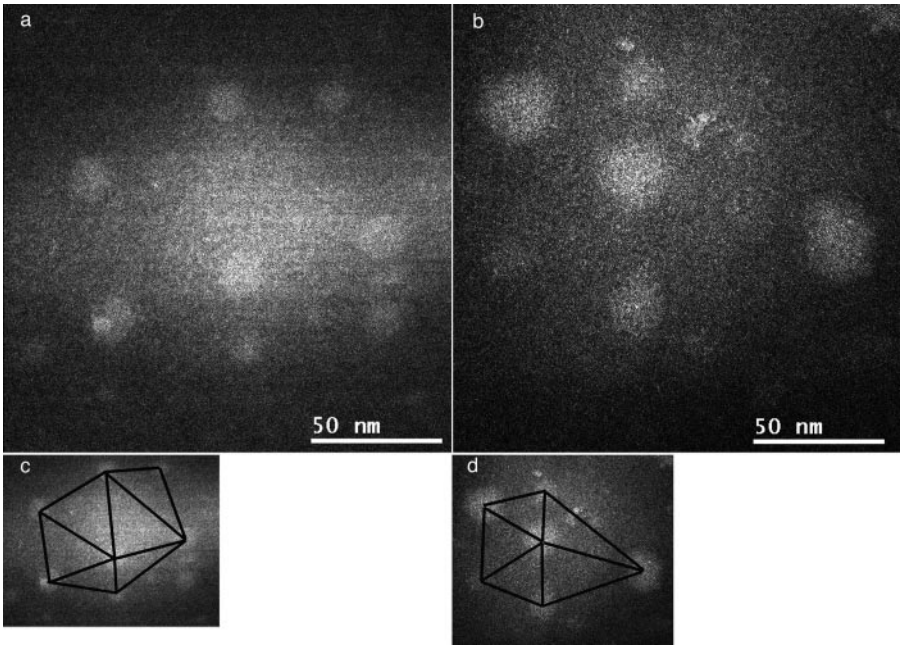

FIGURE 4. **Metabolosome analysis.** *a*, SuperSTEM view of a ultramicrotome section of a whole cell of *E. coli* pAR3114. *b*, SuperSTEM view of a metabolosome fraction from lysed cells. *c*, overlay view of *panel a* showing putative edges of sheets of planar protein linking non-planar structural proteins to form polygonal facets. *d*, overlay view of *panel b* showing putative edges of sheets of planar protein linking non-planar structural proteins to form polygonal facets.

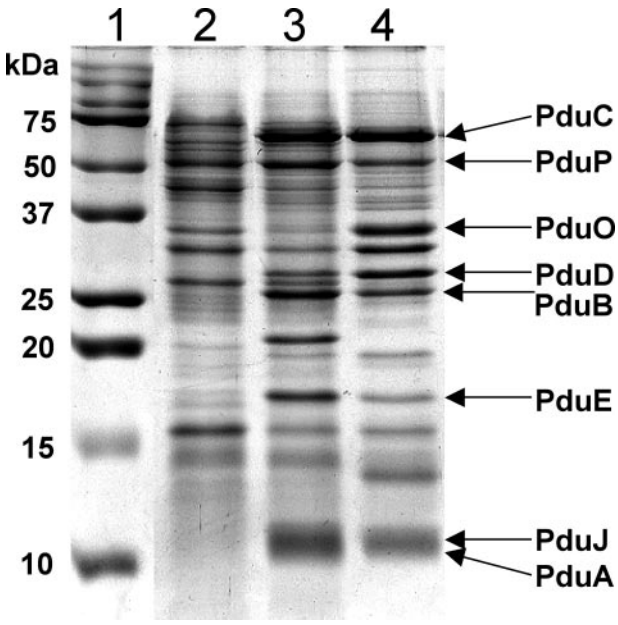

FIGURE 5. **SDS-PAGE analysis of isolated organelle and MALDI-TOF identification of protein components.** Each *lane* contains 10–20 μg of protein, and the gel was stained with Coomassie Blue. *Lane 1*, molecular mass markers; *lane 2*, cell extract of *E. coli* pAR3114 grown in No Carbon E medium + succinate; *lane 3*, cell extract of *E. coli* pAR3114 grown in No Carbon E medium + succinate + 1,2-propanediol; *lane 4*, metabolosomes isolated from *E. coli* pAR3114.

ponent is one (or more) of the three predicted shell proteins, just as minor variants of viral capsid proteins normally forming hexameric sheets form pentameric vertex proteins (28).

Liquid Chromatography-Tandem Mass Spectrometry SDS-PAGE Analysis—To identify proteins present within the metabolosome, purified metabolosome extracts were subjected to SDS-PAGE, and individual protein bands were extracted and analyzed (Fig. 5 and supplemental Table S2). The proteome pattern of metabolosomes isolated from recombinant *E. coli* pAR3114 grown in the presence of 1,2-propanediol is similar to that reported for wild-type *S. enterica* (7). By using MALDI-TOF on trypsin digests of the extracted proteins run out on SDS-PAGE, it was possible to identify PduA,C,D,E,J,O,P as the major components of the recombinant metabolosome. The presence of these proteins as well as PduB′ was further confirmed by two-dimensional gel electrophoresis of the isolated organelle (see supplemental Fig. S1 and Table S2). The 11 major bands seen on the SDS-gel of the purified organelle (Fig. 5) resolved into around 100 spots on the two-dimensional gel, indicating a further layer of complexity. A stoichiometric analysis of the *pdu* organelle proteome from *C. freundii* has yet to be determined. Overall, however, the protein composition of the isolated organelle appears to be similar to the proteomic analysis of the *S. enterica pdu* metabolosome (7).

Two Forms of PduB: B and B′—The *S. enterica* PduB appears to be produced in two forms, one of which is about 5 kDa smaller than the other (7). It was suggested that this was caused by the presence of two translational start sites giving rise to two forms of the protein, referred to as PduB and PduB′ (7). To investigate whether this is also the case in the *C. freundii* Pdu metabolosome, the recombinant production of PduB and B′ from *pduB* was investigated.

Overproduction of the *C. freundii* PduB in *E. coli* was achieved by cloning the gene into pET14b to allow the protein to be produced with an N-terminal His tag. Analysis of the protein profile of the recombinant strain overproducing the *C. freundii* PduB revealed the presence of two major protein bands by SDS-PAGE. When the crude cell extract containing the overproduced PduB was passed through a Ni^{2+} column, both the higher (37 kDa) and lower (32 kDa) molecular mass proteins copurified after elution in imidazole (supplemental Fig. S2*a*). The bands were confirmed as PduB-type proteins by MALDI-TOF analysis after their excision from the SDS-gel and trypsin digestion. Significantly, only the higher molecular mass protein cross-reacted with anti-His tag antibodies when analysed by Western blotting (supplemental Fig. S2*b*). These results are consistent with *pduB* having two translation start sites. The two observed protein bands represent one with an N-terminal His tag and the second one starting at Met-38. The two proteins must form a tight complex, as they were able to copurify on the nickel column. Confirmation of the two start sites was obtained by mutating the codon for Met-38 within *pduB* to Ala (see sup-

plemental material). The resulting protein (PduB only) was produced and purified as a single product (data not shown).

Overproduction of the Shell Proteins, PduA, -B, -J, -K, -T, and -U, in Situ with the Metabolosome Results in Aberrant Structures—Although the absence of *pduA* or *pduB* from the *pdu* operon leads to the loss of metabolosome formation, it was found that overproduction of any one of PduA, -B, B′, -B and -B′, -J, -K, -T, and -U, in a background in which recombinant metabolosomes formed, resulted in significant effects upon size, shape, and aggregation of the organelle (Fig. 6). For overproduction of the individual shell proteins, the relevant gene was cloned into pLys, as described in the supplemental material, a plasmid that is compatible with pED460 (which contains all the *pdu* genes from *pduA* to *pduX*). The pLysS derivative was then transformed into an *E. coli* strain containing pED460 and the resulting derivative analyzed for the presence of cytoplasmic structures. To determine whether the gene product encoded within pLysS was being overproduced *in situ*, cell lysates of the corresponding transformed strains (containing the pLys derivative plus pED460) were analysed. In all but one case, a clear band corresponding to the expected size of the protein could be observed on the SDS-gel at an intensity well above the control strain (supplemental Fig. S3). The one exception was PduU, where no overproduced protein band was seen (supplemental Fig. S3).

Overproduction of PduA within a strain housing pED460 resulted in the appearance of long thin structures in the recombinant *E. coli*, indicating that excess PduA prevents the formation of rounded organelles (Fig. 6*B*). A similar observation had been made previously on PduA overproduction in *S. enterica* (26). Overproduction of PduB and B′ gave large single homogeneous structures with no delimiting feature (Fig. 6*C*). The structure also appeared more granular indicating that too much PduB and B′ prevents normal metabolosome biogenesis. Striking changes in organelle morphology were obtained by the separate overproduction of PduB and PduB′. In the case of the former, large circular bodies were observed containing concentric rings (Fig. 6*D*), whereas with the latter regular straight-lined structures were generated (Fig. 6*E*). From this it would appear that the presence of PduB is important for generating curved structures and that the appropriate level of PduB and PduB′ is important for the shape of the metabolosome. The curvature effect must be a property of the first 38 amino acids present in the N terminus of PduB.

No aberrant structures were observed when *pduA* and *pduB* were expressed together to complement the *pduA,B* knock-out strain. This is likely because the levels of PduA and PduB are low when the two genes are expressed together, in comparison to the much higher levels of protein production that would be expected with the single gene expression studies.

With the overproduction of PduJ, the organelle took on a rosette appearance (Fig. 6*F*). In this case, several layers of (presumably) shell protein produced a whorled architecture. Overproduction of PduK led to the appearance of a single large aggregate complex that still maintained the delimiting substructure feature of individual metabolosomes (Fig. 6*G*). A noticeable change in organelle appearance was observed with attempts to overproduce PduT. Here, cells were either found

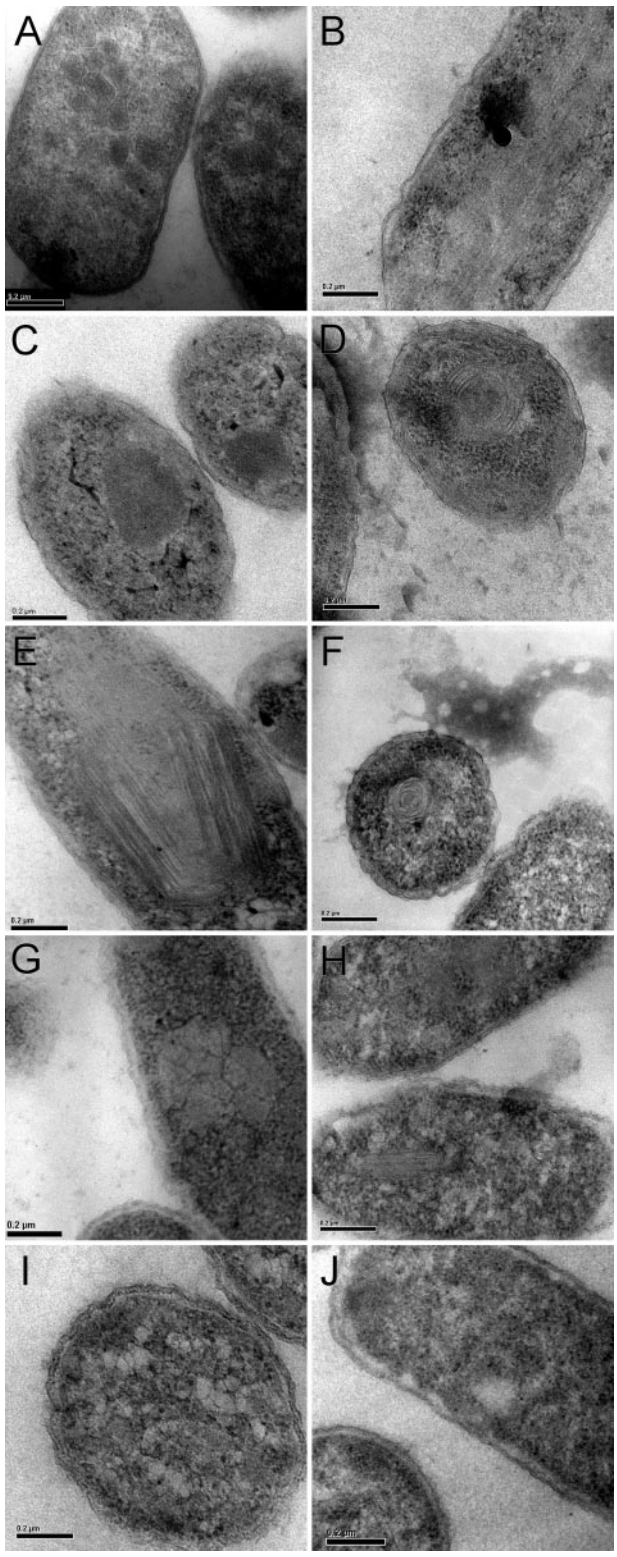

FIGURE 6. **Effect of shell protein overproduction on metabolosome formation.** *A*, a thin section of *E. coli* pAR3114 (housing *pduA-X*) with recombinant metabolosomes. The effect of overproducing certain individual shell proteins within *E. coli* pAR3114 by expressing the respective gene on a separate compatible plasmid is shown in *B–I*. *B* shows the effect of overproducing PduA; *C*, the effect of overproducing PduB and PduB′; *D*, the effect of overproducing PduB; *E*, the effect of overproducing PduB′; *F*, the effect of overproducing PduJ; *G*, the effect of overproducing PduK; *H*, the effect of overproducing PduT; *I*, the effect of overproducing PduU; and *J*, a negative control (*E. coli* containing the empty cosmid vector pLA2914 and pLysS).

with deposits or having lamina-like structures (Fig. 6*H*) not dissimilar to that observed with PduA overproduction, where a layered appearance was observed. When PduU was overproduced, multiple smaller structures were observed, which appeared to clump together (Fig. 6*I*, *J*). In contrast, overproduction of the only remaining putative shell protein, PduN, had no effect upon the appearance of the organelle (data not shown). From these studies it can be concluded that PduA, -B, -B′, -J, -K, -T, and -U play important roles in organelle biogenesis and help to shape the structure. Moreover, the data indicate that organelles require a specific ratio of these shell proteins to orchestrate the correct assembly of the metabolosome.

No structures were observed in strains that contained only the pLysS derivatives. The aberrant organelles were observed only in strains that contained the pLsyS derivatives. Normal organelles were observed when pLysS (with no insert) was transformed into *E. coli* cells containing pED460. Therefore, the changes in organelle morphology must be due to the excess protein encoded within the pLysS derivative.

PduT Contains an Fe-S Center—Overproduction of PduT resulted in the isolation of a brown-colored protein in which the UV-visible spectrum had a broad absorption maximum at 420 nm (Fig. 7*a*), suggesting the presence of an Fe-S center. This was confirmed by EPR analysis, where X-band EPR spectra of PduT (Fig. 7*c*) indicate the presence of a 4Fe-4S iron-sulfur cluster in this protein. The protein as isolated gives rise to a rhombic EPR spectrum at 15 K with $g_{\|} = 1.91$ and $g_{\|} = 2.04$. This spectrum was not visible at 70 K (data not shown). Both of these properties are indicative of the presence of a $[4Fe\text{-}4S]^{1+}$ cluster in the protein as isolated, suggesting that a proportion of the cluster is reduced in the protein under these conditions. Reduction with dithionite increases the amount of $[4Fe\text{-}4S]^{1+}$ detected and confirms the assignment of the signal to a reduced iron-sulfur cluster. The properties of the iron-sulfur cluster suggest that is has a relatively high midpoint redox potential (E_m) and that it is accessible to external redox agents. This was confirmed by redox potentiometry, which revealed that the midpoint potential of the cluster was +99 mV (Fig. 7*b*). Gel filtration analysis (data not shown) suggests that the protein exists as a homotetramer, and as there are less than four conserved cysteines in the protein, the possibility exists that this center is formed from the coordination of several separate subunits.

To investigate further this possibility, we also examined Cys → Ala mutants of the three cysteine residues found in this protein PduT using EPR spectroscopy. Dithionite-reduced proteins (Fig. 8) exhibit the same characteristic $[4Fe\text{-}4S]^{1+}$ EPR spectrum in the C136A and C108A mutants, but this spectrum cannot be obtained for the C38A mutant. This suggests that only one cysteine residue from each PduT protein ligates a 4Fe-4S cluster, a highly unusual arrangement but consistent with the proposed homotetrameric structure. This arrangement may also explain the unusually low $g^{\perp}$ value. Cys-38 is the only cysteine residue conserved in known PduT sequences.

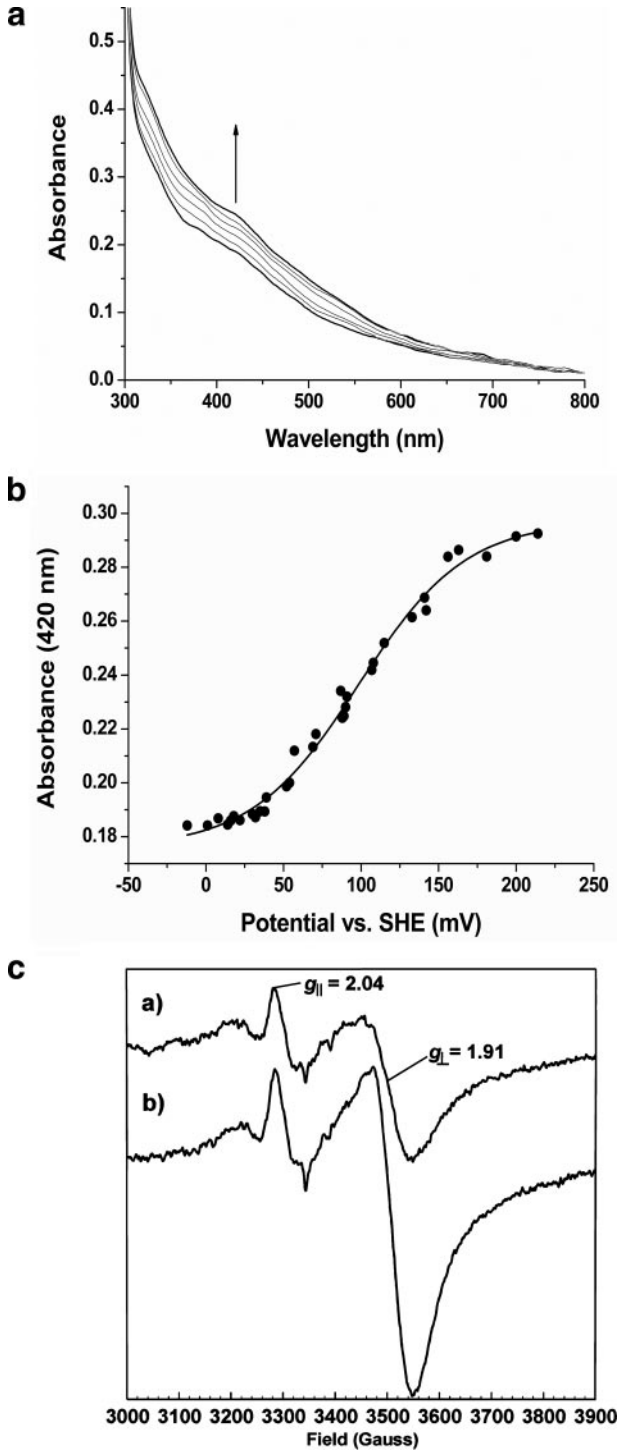

FIGURE 7. **PduT contains an Fe-S center.** *a*, selected set of UV-visible absorption spectra collected during oxidative redox titration of purified PduT with potassium ferricyanide. Redox titration was done as described in the supplemental material. Absorption increases on oxidation of the [4Fe-4S] cluster in the reduction potential range from ~0 to 250 mV (*versus* the standard hydrogen electrode) as indicated by the *arrow*. *b*, a fit of the absorption *versus* potential data (at 420 nm) to a single electron Nernst function, producing a midpoint potential for the $[4Fe\text{-}4S]^{2+}$ to $[4Fe\text{-}4S]^{1+}$ conversion, producing a midpoint potential of 99 ± 3 mV *versus* the standard hydrogen electrode (*SHE*). *c*, X-band EPR spectra of isolated PduT (*spectrum a*) and dithionite-reduced PduT (*spectrum b*). Experimental parameters: microwave power, 0.5 milliwatt; modulation frequency, 100 KHz; modulation amplitude, 5 G; temperature, 15 K.

DISCUSSION

Phylogenetic evidence strongly suggests that horizontal transfer of the propanediol utilization operon has occurred several times in the evolution of the related Enterobacteriaceae,

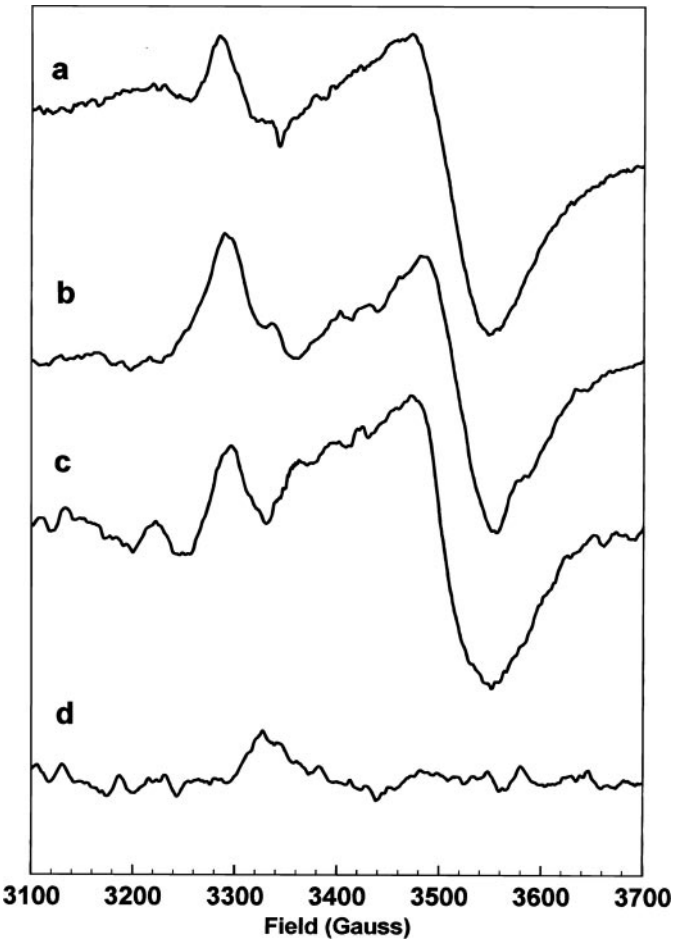

FIGURE 8. **X-band EPR spectra of dithionite-reduced PduT.** The spectra include wild-type PduT (*a*), a C108A variant (*b*), a C136A variant (*c*), and a C38A variant (*d*). Experimental parameters: microwave power, 0.5 milliwatt; modulation frequency, 100 KHz; modulation amplitude, 5 G; temperature, 15 K.

S. enterica and *E. coli* (20, 21), despite the number of genes involved (>20 kb of DNA). We attempted to reproduce this event *in vitro* between *C. freundii* and *E. coli* to show that the complex systems involved were indeed transferable in one step. Electron microscopy of *E. coli* cells carrying plasmids or cosmids harboring the *pdu* genes that had been grown on propanediol medium and not on succinate alone showed polyhedral bodies closely resembling in size and shape those previously reported from other Enterobacteriaceae in which metabolosomes have been induced (3, 6, 7, 29). Assays and protein analysis suggested that these bodies were functioning metabolosomes. In *E. coli* strains containing the cosmid pAR3114, their presence was induced by propanediol and the recombinant host acquired cobalamin-dependent propanediol utilization capacity. In strains carrying pED460, where the regulatory gene had been trimmed, the metabolosomes were constitutively produced.

As for wild-type metabolosomes (7), enzymatic assay of B_{12}-dependent diol dehydratase showed enriched activity in extracted metabolosomes compared with the whole bacterial cell, suggesting concentration of the metabolic enzymes within the organelle. Moreover, the protein components of the purified organelle were found to correspond to the encoded Pdu proteins, thereby confirming the efficacy of the recombinant metabolosome.

The host *E. coli* JM109 contains a functional ethanolamine utilization (*eut*) operon as shown by a standard bioassay (20), implying possession of a set of shell protein genes associated with the *E. coli* ethanolamine utilization operon closely resembling that in *S. enterica* (30). However, no metabolosomes were seen in the control *E. coli* strain that were capable of ethanolamine utilization but lacking *pdu* operon genes when grown on propanediol medium, indicating that these genes were not significantly expressed in propanediol medium. This is the first demonstration that the full functionality of a metabolosome can be horizontally transferred by standard recombinant DNA procedures *in vitro*.

Electron microscopy of extracted recombinant metabolosomes revealed that a high percentage of extracted metabolosomes had ragged surfaces, unlike the previous report in which the surface protein layer was mainly intact (7), even though the metabolosome extracts were fixed prior to negative staining to minimize rupture. This may be because of slight differences in the way the samples were prepared. The dimensions of the extracted organelles were still close to those found for intracellular ones, and the disruption was therefore presumably confined to the surface layer. Apart from this, electron microscopy appearances were similar overall to those reported previously (2, 3, 6, 7), although we noted two features not previously commented on for metabolosomes but recently established in carboxysomes. First, the frequency distribution of metabolosome diameter showed two distinct maxima, suggesting a common elongated nonspherical structural plan. The apparently variable polyhedral appearances seen on electron microscopy may be a combination of fixation artifacts and random cross-sections. Second, a higher intrinsic order within the organelle was detected by FFT, which is compatible with assembly of the organelles from protein subunits of particulate resolution 3.3 and 2.4 nm. A regular substructure is compatible with cryoelectron microscopic studies of *H. neapolitanus* (18) and *Synechococcus* (19) carboxysomes.

It was also observed that an *E. coli* strain carrying a plasmid with the main *C. freundii pdu* genes but deleted in *pduA* and *pduB* had greatly reduced propanediol metabolizing ability. Analysis by electron microscopy of this strain revealed that it had no metabolosomes. However, complementation with a compatible plasmid containing both *pduA* and *pduB* resulted in restoration of full propanediol-utilizing activity and the formation of intracellular organelles. Thus, the presence of the metabolosome appears to enhance the metabolic activity of the organelle-associated enzymes. Furthermore, as the plasmid harboring *pduA* and *pduB*, but not plasmids containing *pduA* or *pduB*, was able to form metabolosomes in this particular *E. coli* strain, it suggests that PduA and PduB are both independently required for metabolosome formation. Moreover, the presence of both PduB and B′ on two-dimensional gels indicates that both proteins are components of the metabolosome.

Organelle formation is dependent upon the appropriate concentration of certain components, as too little or too much of some of the individual proteins can prevent organelle formation or lead to the formation of aberrant structures. Signifi-

cantly, overproduction of PduA, -B, -B′, -B and -B′, -J, -K, -T, and -U, which are all predicted to be shell proteins, in an *E. coli* strain that harbors the *pdu* operon gives rise to abnormal bodies. The differences in shape and form of the organelle when these proteins are overproduced certainly support a role for these proteins in the outer shell of the organelle. The various aberrant organelles were not studied further, and no attempts were made to compare their protein composition with that of wild-type structures. Similarly, no protein localization studies have yet been undertaken to demonstrate whether the putative shell proteins really do form the shell of the structure.

Unexpectedly, isolation of one of these proteins, PduT, revealed that it contained a 4Fe-4S center, with an unusual Cys ligation pattern within a PduT homotetramer, indicating that the organelle has some form of molecular wiring. The presence of such a redox group represents a way by which single electron transfer or redox sensing can be carried out through intact organelle shells without using the structurally established pores or other gaps in the shell proteins. This is an important insight into the metabolic circuitry of the metabolosome, which may also be shared by the carboxysome. It is interesting to note that the cobalamin reductase, PduS, also contains an Fe-S center (31),[6] and thus PduS and PduT could form part of a redox circuit to allow transfer of electrons into the organelle during the reduction of the cobalamin coenzyme. It is also noteworthy that PduS was found to be associated with the isolated metabolosome.

The cloning of the 20-kb *pdu* regulon from *C. freundii* represents a major engineering challenge, on the same scale as the cloning of the cobinamide (*cbi*) biosynthetic region from *S. enterica* into *E. coli* (32). Moreover, it has generated a comparatively simple genetically tractable system to investigate the role of individual components of the propanediol utilization machinery. There is still much to be learned about metabolosomes, such as how the components are pieced together, how the enzymes are internalized, and how substrates and products are moved in and out of the organelle (33). These structures offer the potential for future exploitation in engineered reactions using the organelle architecture to house novel active metabolic processes. Our studies represent the first step toward engineering such systems and toward the rational design of specific prokaryotic cytosolic compartments.

Acknowledgment—We gratefully acknowledge the skillful work done by I. Kristen in transmission electron microscopy sample preparation.

REFERENCES

1. Shively, J. M., Ball, F., Brown, D. H., and Saunders, R. E. (1973) *Science* **182,** 584–586
2. Shively, J. M., van Keulen, G., and Meijer, W. G. (1998) *Annu. Rev. Microbiol.* **52,** 191–230
3. Cannon, G. C., Bradburne, C. E., Aldrich, H. C., Baker, S. H., Heinhorst, S., and Shively, J. M. (2001) *Appl. Environ. Microbiol.* **67,** 5351–5361
4. Shively, J. M., English, R. S., Baker, S. H., and Cannon, G. C. (2001) *Curr. Opin. Microbiol.* **4,** 301–306
5. Heffelfinger, G. S., Martino, A., Gorin, A., Xu, Y., Rintoul, M. D., III, Geist, A., Al-Hashimi, H. M., Davidson, G. S., Faulon, J. L., Frink, L. J., Haaland, D. M., Hart, W. E., Jakobsson, E., Lane, T., Li, M., Locascio, P., Olken, F., Olman, V., Palenik, B., Plimpton, S. J., Roe, D. C., Samatova, N. F., Shah, M., Shoshoni, A., Strauss, C. E., Thomas, E. V., Timlin, J. A., and Xu, D. (2002) *OMICS* **6,** 305–330
6. Bobik, T. A., Havemann, G. D., Busch, R. J., Williams, D. S., and Aldrich, H. C. (1999) *J. Bacteriol.* **181,** 5967–5975
7. Havemann, G. D., and Bobik, T. A. (2003) *J. Bacteriol.* **185,** 5086–5095
8. Shimizu, T., Ohtani, K., Hirakawa, H., Ohshima, K., Yamashita, A., Shiba, T., Ogasawara, N., Hattori, M., Kuhara, S., and Hayashi, H. (2002) *Proc. Natl. Acad. Sci. U. S. A.* **99,** 996–1001
9. Bruggemann, H., Baumer, S., Fricke, W. F., Wiezer, A., Liesegang, H., Decker, I., Herzberg, C., Martinez-Arias, R., Merkl, R., Henne, A., and Gottschalk, G. (2003) *Proc. Natl. Acad. Sci. U. S. A.* **100,** 1316–1321
10. Buchrieser, C., Rusniok, C., Kunst, F., Cossart, P., and Glaser, P. (2003) *FEMS Immunol. Med. Microbiol.* **35,** 207–213
11. Paulsen, I. T., Banerjei, L., Myers, G. S., Nelson, K. E., Seshadri, R., Read, T. D., Fouts, D. E., Eisen, J. A., Gill, S. R., Heidelberg, J. F., Tettelin, H., Dodson, R. J., Umayam, L., Brinkac, L., Beanan, M., Daugherty, S., DeBoy, R. T., Durkin, S., Kolonay, J., Madupu, R., Nelson, W., Vamathevan, J., Tran, B., Upton, J., Hansen, T., Shetty, J., Khouri, H., Utterback, T., Radune, D., Ketchum, K. A., Dougherty, B. A., and Fraser, C. M. (2003) *Science* **299,** 2071–2074
12. Sauvageot, N., Muller, C., Hartke, A., Auffray, Y., and Laplace, J. M. (2002) *FEMS Microbiol. Lett.* **209,** 66–71
13. Prentice, M. B., Cuccui, J., Thomson, N., Parkhill, J., Deery, E., and Warren, M. J. (2003) *Adv. Exp. Med. Biol.* **529,** 43–46
14. Brinsmade, S. R., Paldon, T., and Escalante-Semerena, J. C. (2005) *J. Bacteriol.* **187,** 8039–8046
15. Kerfeld, C. A., Sawaya, M. R., Tanaka, S., Nguyen, C. V., Phillips, M., Beeby, M., and Yeates, T. O. (2005) *Science* **309,** 936–938
16. Tsai, Y., Sawaya, M. R., Cannon, G. C., Cai, F., Williams, E. B., Heinhorst, S., Kerfeld, C. A., and Yeates, T. O. (2007) *PLoS Biol.* **5,** e144
17. Forouhar, F., Kuzin, A., Seetharaman, J., Lee, I., Zhou, W., Abashidze, M., Chen, Y., Yong, W., Janjua, H., Fang, Y., Wang, D., Cunningham, K., Xiao, R., Acton, T. B., Pichersky, E., Klessig, D. F., Porter, C. W., Montelione, G. T., and Tong, L. (2007) *J. Struct. Funct. Genomics* **8,** 37–44
18. Schmid, M. F., Paredes, A. M., Khant, H. A., Soyer, F., Aldrich, H. C., Chiu, W., and Shively, J. M. (2006) *J. Mol. Biol.* **364,** 526–535
19. Iancu, C. V., Ding, H. J., Morris, D. M., Dias, D. P., Gonzales, A. D., Martino, A., and Jensen, G. J. (2007) *J. Mol. Biol.* **372,** 764–773
20. Lawrence, J. G., and Roth, J. R. (1996) *Genetics* **142,** 11–24
21. Porwollik, S., Wong, R. M., and McClelland, M. (2002) *Proc. Natl. Acad. Sci. U. S. A.* **99,** 8956–8961
22. Allen, L. N., and Hanson, R. S. (1985) *J. Bacteriol.* **161,** 955–962
23. Toraya, T., Honda, S., and Fukui, S. (1979) *J. Bacteriol.* **139,** 39–47
24. Munro, A. W., Noble, M. A., Robledo, L., Daff, S. N., and Chapman, S. K. (2001) *Biochemistry* **40,** 1956–1963
25. Ost, T. W., Miles, C. S., Munro, A. W., Murdoch, J., Reid, G. A., and Chapman, S. K. (2001) *Biochemistry* **40,** 13421–13429
26. Havemann, G. D., Sampson, E. M., and Bobik, T. A. (2002) *J. Bacteriol.* **184,** 1253–1261
27. Abrescia, N. G., Cockburn, J. J., Grimes, J. M., Sutton, G. C., Diprose, J. M., Butcher, S. J., Fuller, S. D., San Martin, C., Burnett, R. M., Stuart, D. I., Bamford, D. H., and Bamford, J. K. (2004) *Nature* **432,** 68–74
28. Fokine, A., Leiman, P. G., Shneider, M. M., Ahvazi, B., Boeshans, K. M., Steven, A. C., Black, L. W., Mesyanzhinov, V. V., and Rossmann, M. G. (2005) *Proc. Natl. Acad. Sci. U. S. A.* **102,** 7163–7168
29. Shively, J. M., Bradburne, C. E., Aldrich, H. C., Bobik, T. A., Mehlman, J. L., Jin, S., and Baker, S. H. (1998) *Can. J. Bot. - Rev. Can. Bot.* **76,** 906–916
30. Kofoid, E., Rappleye, C., Stojiljkovic, I., and Roth, J. (1999) *J. Bacteriol.* **181,** 5317–5329
31. Sampson, E. M., Johnson, C. L., and Bobik, T. A. (2005) *Microbiology (Read.)* **151,** 1169–1177
32. Raux, E., Lanois, A., Levillayer, F., Warren, M. J., Brody, E., Rambach, A., and Thermes, C. (1996) *J. Bacteriol.* **178,** 753–767
33. Bobik, T. A. (2006) *Appl. Microbiol. Biotechnol.* **70,** 517–525

[6] J. P. Parsons and M. J. Warren, unpublished material.